JACS
JOURNAL OF THE AMERICAN CHEMICAL SOCIETY
pubs.acs.org/JACS
Article

On the Nature of C(sp^3)−C(sp^2) Bond Formation in Nickel-Catalyzed Tertiary Radical Cross-Couplings: A Case Study of Ni/Photoredox Catalytic Cross-Coupling of Alkyl Radicals and Aryl Halides

Mingbin Yuan,‡ Zhihui Song,‡ Shorouk O. Badir, Gary A. Molander,* and Osvaldo Gutierrez*

Cite This: J. Am. Chem. Soc. 2020, 142, 7225−7234
Read Online
ACCESS | Metrics & More | Article Recommendations | Supporting Information

ABSTRACT: The merger of photoredox and nickel catalysis has enabled the construction of quaternary centers. However, the mechanism, role of the ligand, and effect of the spin state for this transformation and related Ni-catalyzed cross-couplings involving tertiary alkyl radicals in combination with bipyridine and diketonate ligands remain unknown. Several mechanisms have been proposed, all invoking a key Ni(III) species prior to undergoing irreversible inner-sphere reductive elimination. In this work, we have used open-shell dispersion-corrected DFT calculations, quasi-classical dynamics calculations, and experiments to study in detail the mechanism of carbon−carbon bond formation in Ni bipyridine- and diketonate-based catalytic systems. These calculations revealed that access to high spin states (e.g., triplet spin state tetrahedral Ni(II) species) is critical for effective radical cross-coupling of tertiary alkyl radicals. Further, these calculations revealed a disparate mechanism for the C−C bond formation. Specifically, contrary to the neutral Ni-bipyridyl system, diketonate ligands lead directly to the corresponding tertiary radical cross-coupling products via an outer-sphere reductive elimination step via triplet spin state from the Ni(III) intermediates. Implications to related Ni-catalyzed radical cross-couplings and the design of new transformations are discussed.

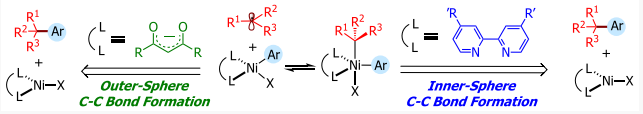

INTRODUCTION

Nickel-catalyzed cross-coupling reactions (CCRs) have emerged as powerful synthetic methods for the mild and selective construction of carbon−carbon bonds.[1] Although C(sp^2)−C(sp^2) couplings are highly reliable and well-established,[2] significant limitations are often encountered in the application of sp^3-hybridized reagents, particularly in the installation of quaternary centers.[3] Notable examples are from reports by the Glorius[4] and Biscoe[5] groups that used a Ni-based catalyst with N-heterocyclic carbene (NHC) ligands to perform C(sp^2)−C(sp^3) cross-couplings between aryl bromides and tertiary alkyl Grignard nucleophiles (Scheme 1A). Fu employed a nickel/bipyridine system for the cross-coupling between unactivated alkyl bromides and organoboron compounds.[6] Gong used a *mono*dentate pyridine as ligand in combination with a nickel system for the reductive coupling between aryl halides and tertiary alkyl halides,[7] while Watson utilized a Ni/phosphine system for the cross-coupling between tertiary benzylic acetates and organoboron compounds.[8] More recently, the Molander group disclosed the first dual photoredox-Ni catalytic strategy for the cross-coupling between potassium tertiary alkyltrifluoroborates and aryl bromides (Scheme 1B).[9] Notably, the *bi*dentate bipyridyl-based ligand (4,4-di-*tert*-butyl-2,2-bipyridine; dtbbpy), which has proven effective in the dual photoredox−Ni-catalyzed cross-coupling of secondary alkylboron reagents, was ineffective with acyclic tertiary alkyltrifluoroborates in this case. On the other hand, *anionic* diketonate-based *bi*dentate ligands (e.g., 2,2,6,6-tetramethyl-3,5-heptanedionate, TMHD, and acetylacetonate, acac) yielded the desired cross-coupling products between *acyclic* tertiary organoboron reagents and a wide range of electron-poor and electron-neutral aryl bromides. In this context, Baran reported the use of an anionic TMHD ligand in the nickel-catalyzed radical C(sp^2)−C(sp^3) cross-coupling between *tertiary* alkyl redox-active esters and arylzinc reagents, while Shenvi reported a dual Mn/Ni(acac)$_2$ system to form all-carbon arylated quaternary centers from tertiary radical precursors.[10]

However, although the evidence for the presence of radical intermediates in these systems is strong,[11] the mechanism, effect of ligand (neutral versus anionic), and molecular-level understanding of the key C(sp^2)−C(sp^3) bond-forming step remain poorly understood. The use of quantum mechanical calculations to investigate the mechanisms, electronic properties, and dynamics of transition metal complexes has led to a deeper understanding of the molecular-level interactions controlling reactivity and selectivity in complex catalytic cycles.[12−17] Herein, quantum mechanical calculations were used to address the following questions: (1) What is the effect

Received: March 3, 2020
Published: March 20, 2020

https://dx.doi.org/10.1021/jacs.0c02355
J. Am. Chem. Soc. 2020, 142, 7225−7234

Scheme 1. Methods for the Construction of All-Carbon Quaternary Centers via Ni-Catalyzed Cross-Couplings between Tertiaryl Alkyl Precursors and Aryl Halides

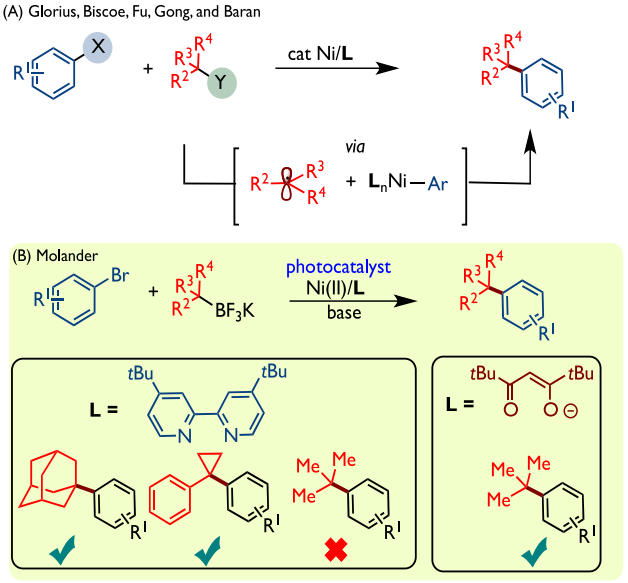

of anionic diketonate-based ligands versus neutral bipyridine ligands in the commonly proposed Ni(0)/Ni(I)/Ni(III) and Ni(0)/Ni(II)/Ni(III) pathways?[17] (2) What are the factors responsible for the distinct reactivity of 2° vs 3° alkyl radicals in the Ni-bipyridine system? (3) What is the role of spin state of the purported Ni complexes and the nature of C(sp^2)−C(sp^3) bond formation in the nickel radical cross-couplings? (4) What is the lifetime of the Ni(III) intermediate prior to undergoing inner-sphere reductive elimination and dynamic effects on radical dissociation/rebound? In this article, we report a comprehensive computational study of the mechanism of Ni-catalyzed CCRs between aryl halides and tertiary alkyl radicals using both neutral (dtbbpy) and anionic (TMHD) ligands with broad implications to related Ni-catalyzed radical cross-couplings involving tertiary alkyl radicals as reported by Fu, Baran, and others.[6,9−11,18]

RESULTS AND DISCUSSION

Methods. All optimizations were performed without restrictions using open-shell, dispersion-corrected DFT (with guess = mix keyword) using THF with the CPCM implicit solvation model [noted as UB3LYP-D3/def2-SVP-CPCM-(THF)] as implemented in Gaussian 09 (see Supporting Information for complete reference). Dispersion correction with Becke−Johnson damping (with EmpiricalDispersion = GD3BJ keyword) was also used to calculate the key pathway in the Ni-bipyridine system, and the results were consistent with those calculated with zero-damping (see Figure S9 in the Supporting Information for comparison of calculated results). Stability tests were conducted (with stable keyword) on all singlet species to confirm that the wave functions are stable as implemented in Gaussian 09, and all singlet species were identified as closed-shell except ^{1}**F′** and ^{1}**G′** based on S^2 values (shown in the Coordinates and Energetics section in the Supporting Information). Further, for comparison and to refine energetics, we also performed single-point energy calculations using a larger basis set (def2-TZVPP), different solvents used experimentally (DMA and THF), other dispersion-corrected DFT functionals (e.g., UM06), and the DLPNO−CCSD(T) method (in ORCA; see Supporting Information for complete reference). These methods have been used extensively to rationalize and predict reactivity and selectivity in transition-metal-catalyzed transformations, including Ni-catalyzed cross-couplings.[13] Overall, all methods lead to the same conclusions (see Supporting Information for details). For simplicity, only the energies obtained from UB3LYP-D3/def2-TZVPP-CPCM (DMA or THF) will be discussed here (see Figure S1 in the Supporting Information for energetics using other methods of the Ni-TMHD system). For all purported intermediates, we considered both low- and high-spin states (i.e., singlet/doublet and triplet/quartet) and performed a manual conformational search to identify the lowest energy structure (see Figure S2 in the Supporting Information). Initially, to reduce the computational cost, we modeled the 2,2,6,6-tetramethyl-3,5-heptanedionate ligand used experimentally (red; Scheme 1B) as acetylacetonate. Notatbly, the acac ligand has also enabled nickel-catalyzed cross-couplings with tertiary radicals albeit with lower yields, as demonstrated by us and Baran.[9,10] Nonetheless, to validate our model, we also compared the lowest energy pathways using the much bulkier TMHD ligand. The calculated energy values and the obtained structures with the TMHD ligand are similar to those using the acac ligand (see Figure S15 in the Supporting Information).

Previously, we used open-shell DFT to investigate the mechanism of the dual photoredox/Ni-catalyzed cross-coupling between aryl bromides and *benzyl radicals*.[17] Therein, we found that the energetically favored pathway, using neutral bipyridine and bisoxazoline ligands, proceeds via facile radical addition to Ni(0) followed by oxidative addition to the aryl halide to form a Ni(III) intermediate [i.e., Ni(0)/Ni(I)/Ni(III) mechanism]. Importantly, although based on the energetics, we could not rule out the Ni(0)/Ni(II)/Ni(III) pathway; we found that both pathways converged to a Ni(III) intermediate, which could undergo reversible radical dissociation/addition prior to undergoing irreversible (and stereodetermining) inner-sphere C(sp^2)−C(sp^3) bond formation. Based on these studies, we first explored the effect of an anionic ligand on the purported mechanisms for comparison (Figure 1).

Ni-TMHD Catalytic System with *tert*-Butyl Radical as Substrate. As shown in Figure 1 (red), in the absence (or low concentration) of alkyl radical, (acac)Ni(I)···substrate complex ^{2}**A** could undergo *facile* oxidative addition via ^{2}**A-TS** (overall barrier is only 4.6 kcal/mol), leading to a Ni(III) ^{2}**B** intermediate (∼11 kcal/mol downhill in energy). We also located a different, slightly higher energy conformation (^{2}**A′-TS**) that permits direct oxidative addition from ^{2}**A′**, after isomerization from ^{2}**A** to complex ^{2}**A′**, to form Ni(III) ^{2}**B** (green-red). In turn, Ni(III) ^{2}**B** will then undergo an internal reorganization from distorted tetrahedral to distorted square planar conformation, leading to Ni(III) ^{2}**C** (uphill in energy by ∼6 kcal/mol from ^{2}**B**).[19] The distorted square planar ^{2}**C** is now poised to undergo facile radical "outer-sphere" cross-coupling with the tertiary alkyl radical. Specifically, in this geometry, the tertiary alkyl radical is energetically favored to complex, but not add, to the Ni center, leading to ^{3}**C-complex**. Finally, this radical will then undergo a spin-selective (barrier is only 3.1 kcal/mol from ^{3}**C-complex**) outer-sphere C(sp^2)−C(sp^3) bond formation (via triplet spin state ^{3}**C-TS**), leading to the desired product and bromo Ni(acac) products (^{3}**P**$_A$ + ***t***-

https://dx.doi.org/10.1021/jacs.0c02355
J. Am. Chem. Soc. 2020, 142, 7225−7234

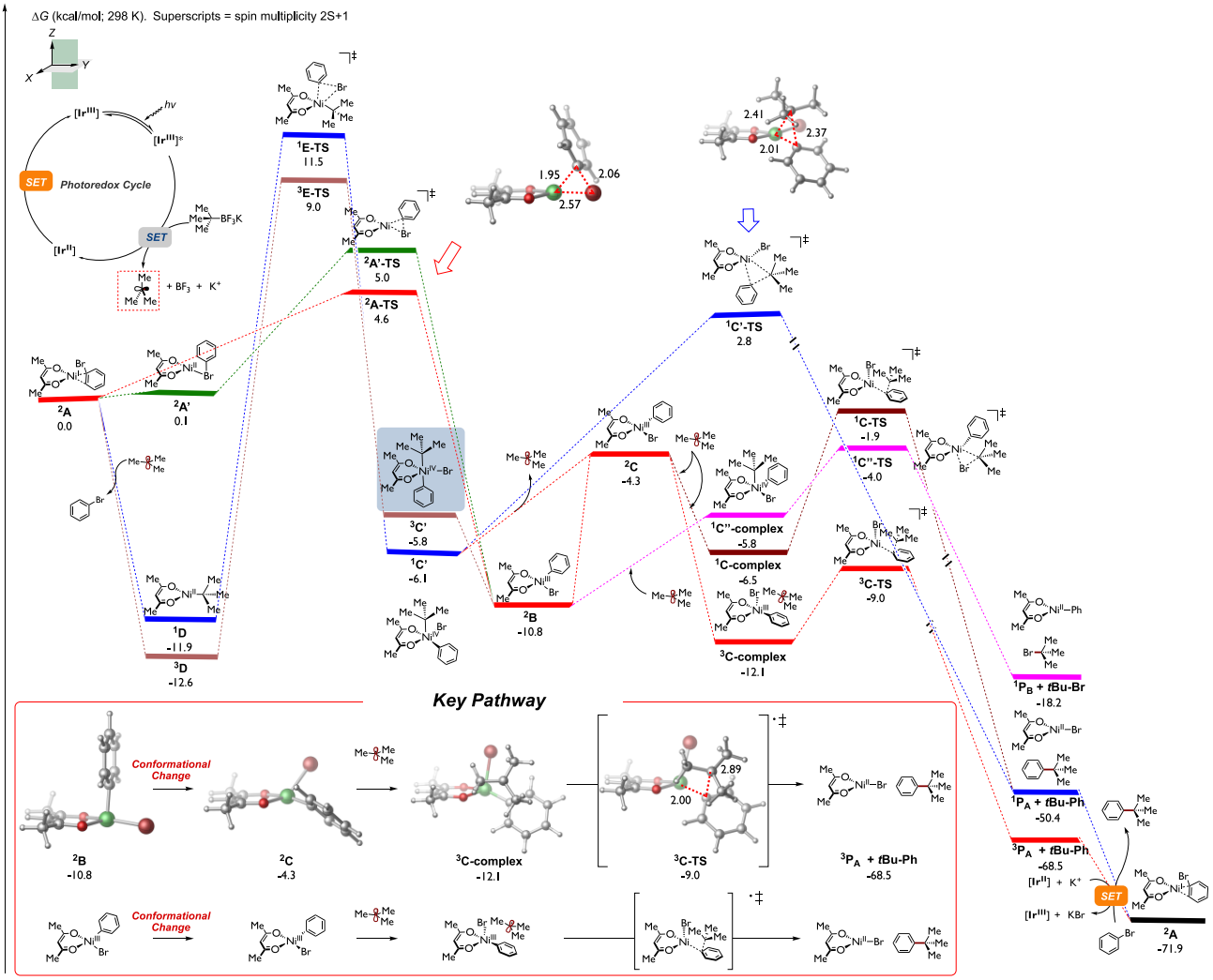

Figure 1. Calculated energetics of the Ni-catalyzed cross-coupling between *tert*-butyl radical and bromobenzene using anionic TMHD as ligand. Relative Gibbs free energy values were computed at the UB3LYP-D3/def2-TZVPP-CPCM(DMA)//UB3LYP-D3/def2-SVP-CPCM(THF) level.

Bu-Ph) downhill in energy by ~69 kcal/mol. ^{3}**P$_A$** will then undergo an energetically favorable single electron transfer (SET) with the photocatalyst ([**Ir^{III}**] = [Ir{dFCF$_3$ppy}$_2$(bpy)]$^+$) to generate the nickel catalyst ^{2}**A** with concomitant formation of KBr complex to restart the transition metal catalytic cycle (see Figure S17 in the Supporting Information for details).

Notably, the outer-sphere radical coupling via the singlet spin state (^{1}**C-TS**) is found to be ~7 kcal/mol higher in energy than the calculated ^{3}**C-TS** and is thus not productive.[14] We also explored alternative pathways initiated from radical addition to the phenyl bromide Ni(acac) complex ^{2}**A**, but all were found higher in energy. Specifically, as shown in Figure 1 (light brown), in the presence of alkyl radical, radical addition to ^{2}**A** and concomitant displacement of phenyl bromide could lead to singlet ^{1}**D**, which is exergonic by ~12 kcal/mol. The triplet spin state (^{3}**D**) is also favored by more than 12 kcal/mol. From ^{3}**D**, calculations predict a high-barrier (~22 kcal/mol) and rate-determining, oxidative addition via triplet spin state (^{3}**E-TS**), leading to ^{3}**C′**. Unexpectedly, this ^{3}**C′** intermediate will then undergo barrierless tertiary radical dissociation, leading back to distorted tetrahedral ^{2}**B**, merging both pathways. Alternatively, ^{3}**C′** could undergo an intersystem crossing (^{3}**C′** → ^{1}**C′**; not calculated) followed by radical dissociation leading back to distorted square planar ^{2}**C** intermediate. Ultimately, both of these pathways will lead to triplet spin, outer-sphere C(sp^2)−C(sp^3) bond formation (via ^{3}**C-TS**). Based on prior computational studies by us and others,[13−17] we also considered the possibility of the commonly proposed singlet spin state, inner-sphere reductive elimination (^{1}**C′-TS**) that can be directly accessed from ^{1}**C′**. However, this pathway was found much higher in energy (~12 kcal/mol) than the triplet spin, outer-sphere C(sp^2)−C(sp^3) bond formation, and thus this pathway, with an anionic diketonate ligand, can be ruled out. In addition, based on our prior work in Fe-catalyzed radical cross-couplings,[20] we also located (pink) the reductive elimination transition state (^{1}**C″-TS**) and the corresponding Ni-tertiary alkyl intermediate ^{1}**C″-complex**, which leads to the formation of tertiary alkyl bromide (***t*-Bu-Br**) and phenyl Ni(acac) (^{1}**P$_B$**). However, this pathway was also found to be higher in energy and thus unproductive. Nonetheless, akin to Ni(I)−Ar intermediates invoked in related cross-coupling reactions,[6] in principle, LNi-Ph (^{1}**P$_B$**) could undergo oxidative addition to the tertiary alkyl bromide (reverse reaction, the barrier is only ~14 kcal/mol), leading to ^{1}**C″-complex**. In turn, these complex computational results also predict radical dissociation to form distorted ^{2}**B**

https://dx.doi.org/10.1021/jacs.0c02355
J. Am. Chem. Soc. 2020, 142, 7225−7234

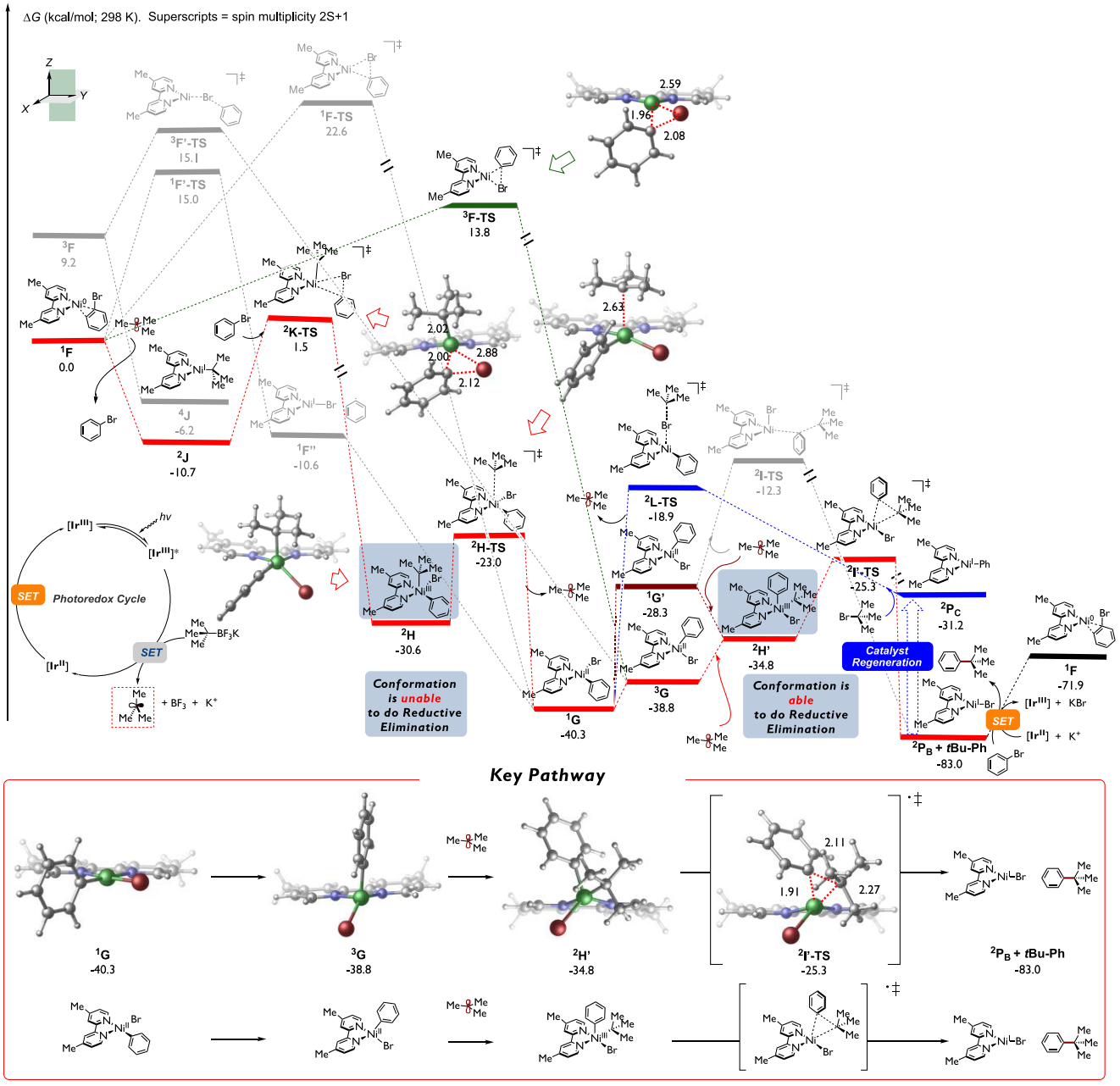

Figure 2. Calculated energetics of the Ni-catalyzed cross-coupling between *tert*-butyl radical and bromobenzene using neutral bipyridine as ligand. Relative Gibbs free energy values were computed at the UB3LYP-D3/def2-TZVPP-CPCM(THF)//UB3LYP-D3/def2-SVP-CPCM(THF) level of theory.

and, ultimately, lead to outer-sphere C(sp^2)−C(sp^3) bond formation. Thus, independent of active nickel species (LNi, LNi-alkyl, or LNi-aryl; L = acac), these calculations revealed a new mechanistic manifold in which tertiary alkyl radicals involved in Ni-diketonate systems are predicted to proceed via outer-sphere C(sp^2)−C(sp^3) bond formation via a triplet spin state. We also considered the likelihood of explicit DMA solvent coordinating to the key nickel species ^{2}**A** or ^{2}**C** and promoting ligand dissociation. However, calculations showed that the DMA solvent is unlikely to cause ligand dissociation during the transition metal catalytic cycle (see Figure S14 in the Supporting Information). Moreover, we also carried out experiments using excess TMHD anionic ligand (see Supporting Information). These results showed that excess TMHD ligand (50 and 100 mol %), which would coordinatively saturate the nickel intermediates, has a minor effect on the efficiency of the system (*vide infra*). Finally, the electronic properties of the aryl bromide do not change the overall mechanistic conclusions (see Figure S3 in the Supporting Information).

Overall, as shown in Figure 1 (inset), the key findings from calculations are summarized as follows: For anionic diketonate-Ni systems involving tertiary alkyl radicals (i.e., as reported by Molander,[9] Baran,[10a] and Shenvi[10b]) after oxidative addition from Ni(I) complex ^{2}**A**, distorted tetrahedral Ni(III) species ^{2}**B** can be formed, which requires a conformational change to form the distorted square planar ^{2}**C**. Subsequently, ^{2}**C** can form the triplet spin ^{3}**C-complex** with a tertiary alkyl radical, followed by a triplet spin, outer-sphere C(sp^2)−C(sp^3) bond-forming pathway via ^{3}**C-TS** to generate the desired product

https://dx.doi.org/10.1021/jacs.0c02355
J. Am. Chem. Soc. 2020, 142, 7225−7234

and bromo Ni(acac) (^{3}**P$_A$** + ***t*-Bu-Ph**). In sum, independent of mechanism, in the presence of tertiary alkyl radicals, these results strongly support a novel, low-barrier, spin-selective "outer-sphere" radical cross-coupling pathway via triplet spin state and, contrary to commonly proposed pathways, disfavor the formation of sterically hindered halo-aryl-alkyl-Ni intermediates using anionic ligands.[21] These results could be applied to a wide range of experimental observations in which privileged anionic ligands, in combination with nickel complexes, allow radical cross-coupling with tertiary radical precursors.[9,10]

Ni-Bipyridine Catalytic System with *t*-Bu Radical Substrate. Previously, neutral bipyridine ligands in combination with nickel as catalyst failed to undergo C(sp^2)−C(sp^3) cross-couplings with acyclic tertiary radical under dual photoredox/nickel catalysis (Scheme 1B). Nonetheless, this bipyridyl-nickel system has found success for a wide range of Ni-catalyzed radical C(sp^2)−C(sp^3) cross-couplings with secondary and cyclic tertiary alkyl radical precursors, and many groups, including ours,[13c,17,22c] have taken advantage of this reactivity to promote selective dicarbofunctionalization of olefins.[16,22] However, despite the widespread utility of the bipyridyl-nickel system in organic synthesis with tertiary alkyl radicals, the mechanism and, in particular, the nature of the critical C−C bond formation is not known. To gain insights from this divergent reactivity with tertiary alkyl radicals, we examined the competing reaction pathways (Figure 2, see Figure S4 in the Supporting Information for energetics using other methods).

Ni(0)/Ni(I)/Ni(III) Pathway. As with previous calculations, in the presence of alkyl radical, overall the lowest energy pathway (red) proceeds via barrierless *tert*-butyl radical addition to Ni(0), leading to Ni(I) intermediate ^{2}**J**. In turn, Ni(I) ^{2}**J** undergoes oxidative addition to aryl halide via ^{2}**K-TS**; the overall barrier is ∼12 kcal/mol from ^{2}**J**, leading to Ni(III) intermediate ^{2}**H**. However, despite numerous attempts, we were unable to locate the direct, inner-sphere reductive elimination from this isomer. Instead, we found a very low barrier tertiary alkyl radical dissociation (via ^{2}**H-TS**) that leads to the formation of square planar Ni(II) intermediate ^{1}**G**. This square planar aryl halide Ni(II) intermediate is favored to undergo an intersystem crossing/conformational change to form the tetrahedral, triplet spin state Ni(II) intermediate ^{3}**G**. In turn, ^{3}**G** is now poised to undergo radical addition to form Ni(III) intermediate ^{2}**H′** followed by inner-sphere reductive elimination (via ^{2}**I′-TS**), leading to the desired products ^{2}**P$_B$** and ***t*-Bu-Ph**, which is exergonic by 83 kcal/mol. After the C(sp^2)−C(sp^3) bond-forming step, SET can occur between the bromo Ni species and the reduced Ir photocatalyst to regenerate the Ni(0) catalytic species ^{1}**F** with concomitant formation of KBr complex and restart the transition metal catalytic cycle (see Figure S17 in the Supporting Information for details). Overall, catalyst regeneration is ∼11 kcal/mol uphill in energy but, based on the free energy span, energetically favorable. Given the prevalence of proposed Ni(I)/Ni(III)/Ni(I) pathways by the community and the lack of understanding of the dynamic effects in nickel-catalyzed radical cross-coupling reactions, we conducted preliminary quasi-classical dynamics simulations on the transition state of oxidative addition ^{2}**K-TS** and that of reductive elimination ^{2}**I′-TS**, respectively (see Figure S13 in the Supporting Information). Simulated results suggest that starting from ^{2}**K-TS** in the forward direction, 60% of the trajectories resulted in the formation of a Ni(III) intermediate, while 40% formed the square planar Ni(II) intermediate and concomitant dissociation of *tert*-butyl radical. No cross-coupling product (*t*-Bu-Ph) was observed in any simulated trajectory (see Figure S13a in the Supporting Information for details). These observations support our static DFT calculations that the Ni(III) intermediate obtained from direct oxidative addition on the alkyl Ni(I) intermediate cannot undergo reductive elimination, but rather undergoes radical dissociation to generate the square planar Ni(II) intermediate ^{1}**G**. On the other hand, within dynamics calculations propagated from ^{2}**I′-TS** in the reverse direction, all trajectories ended up in the Ni(III) intermediate without radical dissociation from the Ni center or structural rearrangement (see Figure S13b in the Supporting Information for details). This is also consistent with our assumption concerning the overall process because the radical addition to Ni involves a change of spin state of the Ni(II) species, while quasi-classical dynamics simulations only operate in a single spin state.[23] From a broader perspective, these results suggest a novel Ni(0)/Ni(I)/Ni(III)/Ni(II)/Ni(III)/Ni(I) pathway in bipyridine-nickel radical cross-couplings with tertiary alkyl radicals.

Ni(0)/Ni(II)/Ni(III) Pathway. In the absence (or low concentration) of a *tert*-butyl radical, Ni(0) could undergo oxidative addition via the triplet spin state (^{3}**F-TS**; green), leading directly to the productive tetrahedral, triplet spin state Ni(II) ^{3}**G** intermediate, thus merging both Ni(0)/Ni(I)/Ni(III)/Ni(II) (red) and Ni(0)/Ni(II) (green) pathways. We also considered the possible outer-sphere C−C bond formation pathway between *tert*-butyl radical and Ni(II) intermediate, but the transition states of both the doublet (^{2}**I-TS**) and quartet spin state pathways (^{4}**I-TS**) are higher in energy compared to ^{2}**I′-TS** (see Figure S4 in the Supporting Information for details). Therefore, inner-sphere reductive elimination via Ni(III) intermediate ^{2}**H′** is preferred to that of the outer-sphere pathway from the Ni(II) intermediate in Ni-bipyridine catalytic systems.

Ni(I)/Ni(II)/Ni(III) Pathway. Previously, alkyl halide activation by Ni(I) species (akin to ^{2}**Pc**) have been proposed in a range of Ni-catalyzed cross-couplings.[24] As shown in Figure 2 (blue), in these cases, aryl bipyridine-Ni(I) could undergo halogen abstraction (via ^{2}**L-TS**; barrier ∼12 kcal/mol from ^{2}**Pc**), leading to the Ni(II) ^{1}**G**, thus also merging the cross-coupling cycles. Finally, Ni(II) ^{1}**G** will need to undergo an isomerization/spin-crossing to form the productive tetrahedral Ni(II) ^{3}**G**, which, after barrierless radical addition, will form the productive Ni(III) ^{2}**H′**. Finally, inner-sphere reductive elimination (via ^{2}**I′-TS**) will lead to the desired product and bromo Ni(I). From a broader perspective, although the pathway for catalyst regeneration from the bromo Ni(I) varies among nickel-catalyzed cross-coupling methods [e.g., it could undergo SET by photocatalyst or external reductant to form a Ni(0) ^{1}**F** or, alternatively, could undergo transmetalation to form the Ni(I) ^{2}**P$_{C6}$**], calculations show that these systems involving tertiary alkyl radicals share the same critical C(sp^2)−C(sp^3) formation step! As an example, the phenyl bpy-Ni(I) species was proposed to be obtained via transmetalation in Fu's experiments.[6] The overall key findings of these calculations are summarized as follows (Figure 2; inset): after singlet spin square planar Ni(II) species ^{1}**G** forms, this species needs to undergo intersystem crossing/conformational change to generate the triplet spin tetrahedral ^{3}**G** complex followed by tertiary alkyl radical addition to form Ni(III)

https://dx.doi.org/10.1021/jacs.0c02355
J. Am. Chem. Soc. 2020, 142, 7225−7234

intermediate ^{2}**H′** (see Figure S6 in the Supporting Information for more detailed analysis). The requirement for the tetrahedral Ni(II) conformation to undergo Ni(II)/Ni(III) radical addition was also reported in a recent paper with a neutral bis(oxazoline) ligand, in which phenyl bromo Ni(II)-bis(oxazoline) is in a square planar geometry, while the radical adds to a tetrahedral phenyl bromo Ni(II) species.[13e] Moreover, the results of our preliminary quasi-classical dynamics calculation are consistent with this suggested pathway (see Figure S7 and Figure S8 in the Supporting Information). Finally, ^{2}**H′** will undergo a doublet spin, inner-sphere reductive elimination pathway via ^{2}**I′-TS** to generate the desired C(sp^2)−C(sp^3) cross-coupling product and bromo Ni(bipyridine) (^{2}**P$_B$** + ***t*-Bu-Ph**).

Origin of the Difference in the C(sp^2)−C(sp^3) Bond-Forming Step in Ni-TMHD and Ni-Bipyridine Catalytic Systems. As shown above, independent of the operative catalytic active species, all pathways converge at the Ni(II) and tertiary radical. Thus, assuming facile intersystem crossing/conformational change, the barrier for inner-sphere tertiary radical C(sp^2)−C(sp^3) cross-coupling using the neutral bipyridine nickel system (∼15 kcal/mol from ^{1}**G**) is much higher in energy than using an anionic diketonate nickel system (∼4 kcal/mol). These relative barriers are consistent with the experiments that prevented the formation of the desired C(sp^3)−C(sp^2) bond using acyclic tertiary radicals under the Ni-bipyridyl/PC system.[9] Moreover, the higher barrier could lead to unwanted side reactions with tertiary radicals such as H atom abstraction from the solvent, as observed by us.[9,25] Further, in accord with experiments by Fu,[6] switching to solvent systems with high bond dissociation energies (BDEs) (e.g., benzene) likely increases the barrier for H-abstraction and, in turn, allows favorable kinetics to promote C(sp^3)−C(sp^2) bond formation with tertiary alkyl radicals. The competence of alkyl radical undergoing H-abstraction (e.g., with solvent or other reagents) or C(sp^3)−C(sp^2) bond formation is not only seen in the Ni-bipyridine system in Fu's report[6] but also observed in the Ni-TMHD(acac) system,[10] suggesting that the H-abstraction reactions with alkyl radical are competing with C−C bond formation in related cross-coupling reactions and the efficiency of C−C bond formation (e.g., H-abstraction versus C−C cross-coupling) is likely system dependent.

On the other hand, the cross-coupling barrier for the diketonate-nickel system is only ∼3 kcal/mol from the respective nickel complex and tertiary alkyl radical. Thus, we attribute the efficiency of Ni-diketonate systems with tertiary alkyl radicals under photocatalytic conditions[9,10] to the nature of the outer-sphere C−C bond formation that avoids the formation of a high-energy, sterically congested aryl-alkyl-halo-Ni intermediate. Experiments using less sterically hindered secondary alkyltrifluoroborates also led to the desired product in 95% yield (Scheme 2). However, in contrast to tertiary alkyl radicals, through DFT calculations we found that the favored pathway for less sterically secondary alkyl radicals is via inner-sphere C−C bond formation with overall barriers for C−C bond formation of ∼9 kcal/mol (see Figure S21 in the Supporting Information). Presumably, the less sterically hindered secondary alkyl radical (in contrast to the tertiary alkyl radical) does not pay a penalty to form the aryl-alkyl-halo-Ni species and can quickly undergo inner-sphere C−C bond formation. In contrast to the bipyridyl-Ni system, these results suggest that for acac/TMHD-Ni systems, the nature of the C−C bond formation and whether inner- or outer-sphere C(sp^2)−C(sp^3) is operative are dependent on the steric properties of the alkyl radical. Surprisingly, for cyclic tertiary systems, we found that this system did not undergo aryl substrate activation in the experiment, leading, after 24 h, to the recovered starting material (see Supporting Information). Although the reasons for lack of reactivity are not completely understood, computations showed that, if the cyclic radical were to engage with the nickel in the cross-coupling cycle, the formation of 1-bromoadamantane via inner-sphere C−Br bond formation is favored over C−C bond formation (see Figure S22 in the Supporting Information). However, because substoichiometric additives (e.g., LiBr, $ZnBr_2$, $ZnCl_2$) were found to influence the reactivity of substrates in the Ni-TMHD system where the bicyclic substrate (adamantyl-like) also failed,[10] the exact reason for the failure of the adamantyl substrate remains unknown and is under exploration in our group.

To understand more fully the origins of the distinct reactivity (i.e., ligand effect on C−C bond formation), we conducted an activation strain-distortion/interaction analysis.[26] As shown in Table 1, comparing inner-sphere and outer-sphere C−C bond formation transition states in the Ni-bipyridine catalytic system (green background), the relative activation electronic energy of inner-sphere transfer is negative (−3.9 kcal/mol) while that of outer-sphere transfer is positive, meaning that the C−C bond formation is favorable via an inner-sphere pathway (see Table S1 in the Supporting Information for energetics using other methods). Despite the

Scheme 2. Cross-Coupling of Secondary Alkyltrifluoroborates with Ni-TMHD

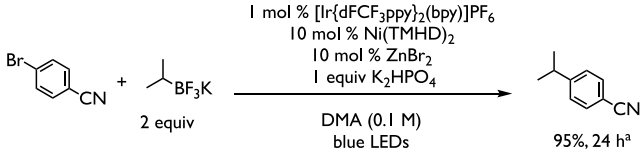

Table 1. Activation Strain-Distortion/Interaction Analysis of the C(sp^2)−C(sp^3) Bond Formation Step[a]

		$\Delta E_{activation}$ (kcal/mol)	$\Delta E_{distortion}$ (kcal/mol)	$\Delta E_{interaction}$ (kcal/mol)
Outer-Sphere	^{2}**I-TS**	19.1	28.6	-9.6
	^{4}**I-TS**	12.2	17.1	-4.9
Inner-Sphere	^{2}**I′-TS**	-3.9	41.0	-44.9
Outer-Sphere	^{1}**C-TS**	2.7	16.0	-14.0
	^{3}**C-TS**	-13.3	18.4	-31.7
Inner-Sphere	^{1}**C′-TS**	-13.2	20.8	-34.0

[a]Relative electronic energy values were computed with respect to the separate corresponding phenyl-bromo-Ni-ligand species and *tert*-butyl radical at the UB3LYP-D3/def2-TZVPP//UB3LYP-D3/def2-SVP-CPCM(THF) level of theory.

https://dx.doi.org/10.1021/jacs.0c02355
J. Am. Chem. Soc. 2020, 142, 7225−7234

Table 2. Analysis of Distinct Alkyl Radical Reactivity in the Ni-Bipyridine System[a]

	ΔG (kcal/mol; 298K) 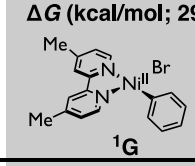 ¹G	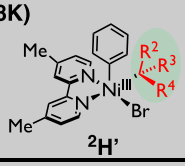 ²H′	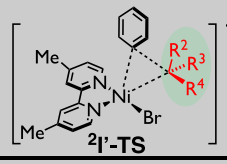 ²I′-TS	BDE of Ni-C(sp³) (ΔH; kcal/mol)	$\Delta E_{activation}$ (kcal/mol)	$\Delta E_{distortion}$ (kcal/mol)	$\Delta E_{interaction}$ (kcal/mol)
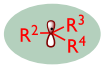		5.6	15.0	11.0	-3.9	41.0	-44.9
	0.0	-2.3	4.2	18.3	-13.9	37.4	-51.2
		-3.4	2.7	17.9	-14.2	33.1	-47.3
		-3.3	7.3	18.3	-8.0	32.4	-40.4

[a]Gray: calculated energetics on the inner-sphere reductive elimination step with different alkyl radicals. Green: related analysis on bond dissociation energy of the Ni(III) intermediate. Yellow: activation strain-distortion/interaction analysis on the reductive elimination transition state [relative electronic energy values were calculated with respect to the separate corresponding Ni(II) species and *tert*-butyl radical]. Relative free energy values were computed concerning the Ni(II) species at the UB3LYP-D3/def2-TZVPP-CPCM(THF)//UB3LYP-D3/def2-SVP-CPCM(THF) level of theory; bond dissociation energy and relative electronic energy values were calculated at the UB3LYP-D3/def2-TZVPP//UB3LYP-D3/def2-SVP-CPCM(THF) level of theory.

larger distortion energy of the inner-sphere compared to the outer-sphere pathway, its interaction energy compensates for the larger distortion energy and makes the overall process favorable. On the other hand, for the Ni-TMHD system (blue background) both inner-sphere and outer-sphere transition states possess negative activation electronic energies, and both their distortion energy and interaction energy are close to each other. Although the inner-sphere and outer-sphere pathways of the Ni-TMHD system do not show as large a difference as those of the Ni-bipyridine system, the triplet spin state outer-sphere pathway is still found most favorable (−13.3 kcal/mol) because of its lower distortion energy (18.4 kcal/mol) and larger interaction energy (−31.7 kcal/mol).

Origin of Distinct Alkyl Reactivity in the Ni-Bipyridine System. Because of the observed experimental differences of structurally different alkyl radicals in Ni-bipyridine systems,[9] we became interested in exploring the potential reactivity of different alkyl radicals in the above key pathways (Table 2). Specifically, in the dual photoredox-Ni catalytic system, $C(sp^2)-C(sp^3)$ cross-coupling succeeded with aryl bromides as the electrophile and potassium 1-adamantyltrifluoroborate and potassium 1-phenylcyclopropyltrifluoroborate as the nucleophile (Scheme 1B).[9] Therefore, we compare here the reactivity of the *tert*-butyl radical, isopropyl radical, 1-phenylcyclopropyl radical, and 1-adamantyl radical in the key inner-sphere reductive elimination step (see Figure S6 in the Supporting Information for the comparison of different radicals in other steps). As shown in Table 2 (gray), using distinct Ni(II) species **¹G** and the purported alkyl radicals as a reference, we observed that the relative energy values of Ni(III) **²H′** intermediates, which are reactive toward inner-sphere reductive elimination, vary for different alkyl radicals. First, we observed that the Ni(III) intermediate with the *tert*-butyl radical (black) is endergonic by 5.6 kcal/mol, while all other Ni(III) intermediates with tertiary and secondary alkyl radicals (red, blue, and green) are exergonic (by 2−3 kcal/mol). These results suggest that the *tert*-butyl radical is more favorable to dissociate from the Ni(III) center to form Ni(II) and a *tert*-butyl radical, while for the other tertiary and secondary alkyl radicals the energetics favor the formation of a Ni(III) complex. This trend is also observable in the barriers for reductive elimination. Specifically, the barriers for inner-sphere reductive elimination of cyclic and secondary alkyl radicals are significantly lower (by 7−12 kcal/mol) than with the *tert*-butyl radical. This observation is consistent with the results in experiments by Fu, where 1-iodoadamantane, with the assumption of the 1-adamantyl radical being generated *in situ*, can also be cross-coupled under nonphotocatalytic condition despite their slightly higher barrier of reductive elimination (7.3 kcal/mol) compared to a secondary isopropyl radical.[6]

Further, to gain insight into the observed trends, we computed the BDE of the $Ni-C(sp^3)$ bond with different alkyl radicals. As shown in Table 2 (green), we found that the Ni−C(*tert*-butyl) bond has the lowest BDE (11.0 kcal/mol), which indicates that the dissociation of the *tert*-butyl radical from the Ni(III) center is easier than the dissociation of secondary and cyclic tertiary alkyl radicals (∼18 kcal/mol). Also, from an activation strain-distortion/interaction analysis on the reductive elimination step (yellow), we found that the transition state with the *tert*-butyl radical shows a less negative activation energy and larger distortion energy compared to the rest of the systems. This suggests that reductive elimination with the *tert*-butyl radical is less favorable because it needs to pay a higher energy penalty for distortion to reach the geometry in the $C(sp^2)-C(sp^3)$ bond-forming step. Although the exact mechanism of bipyridyl-nickel-involved radical cross-coupling reactions could be significantly different depending on the experimental condition and applied substrates/additives, our findings on the nature of $C(sp^2)-C(sp^3)$ bond formation can be used to explain some of the observed selectivity in the selective dicarbofunctionalization of olefins with a broad variety of secondary and tertiary alkyl radical precursors.[13c,16,17,22]

CONCLUDING REMARKS

In summary, quantum mechanical calculations and quasi-classical direct dynamics simulations have been used to investigate the mechanism of dual photoredox-Ni-catalyzed $C(sp^2)-C(sp^3)$ cross-coupling reactions between tertiary

https://dx.doi.org/10.1021/jacs.0c02355
J. Am. Chem. Soc. 2020, 142, 7225−7234

alkyltrifluoroborates and aryl halides with Ni bipyridine- and diketonate-based catalytic systems. Calculations showed the prominent effect of the charge on the ligand on key catalytic intermediates and the C(sp^2)−C(sp^3) bond-forming step in such transformations. Specifically, as outlined in Scheme 3, in

Scheme 3. Catalytic Cycle for Photoredox/Ni Dual Catalytic System Using (A) Neutral (Blue) and (B) Anionic (Red) Ligands

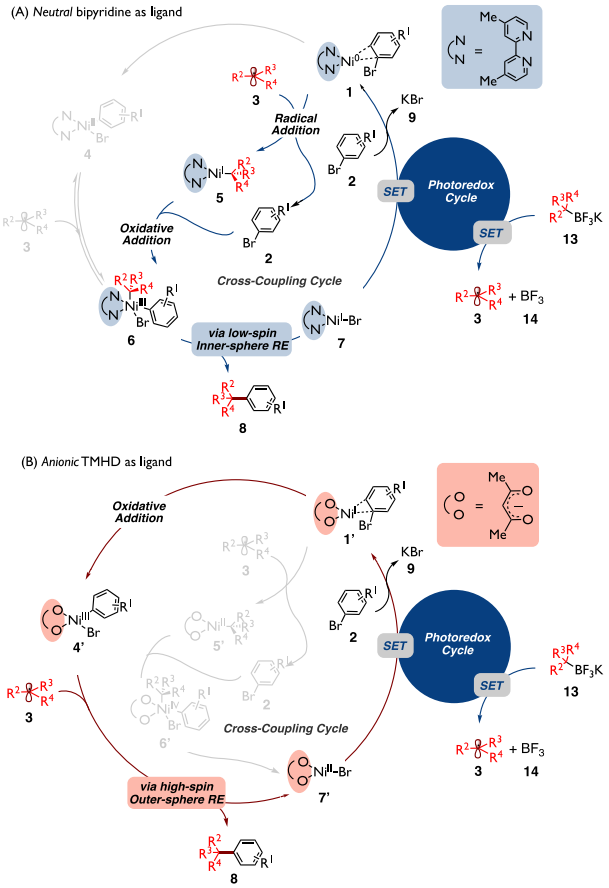

the Ni-TMHD (anionic ligand) system, the tertiary alkyl radical can directly interact with the aryl-bromo-Ni species to obtain the desired product via a high-spin, outer-sphere reductive elimination pathway without engaging the Ni center first. In the Ni-bipyridine (neutral ligand) system, as shown by transition state calculations and supported by quasi-classical dynamics, the Ni(III) intermediate directly obtained from oxidative addition on alkyl Ni(I) species needs to undergo radical dissociation to form the singlet-spin square planar Ni(II) intermediate. Then, it needs to undergo a conformational change/intersystem crossing followed by radical addition to gain access to the productive *tetrahedral triplet spin state* Ni(III) intermediate, followed by subsequent low-spin, inner-sphere reductive elimination to generate the desired product and halide Ni(I). From a broader perspective, although the pathway for catalyst regeneration from the halide Ni(I) varies among different nickel-catalyzed cross-coupling methods [e.g., it could undergo SET by photocatalyst or external reductant to form a Ni(0) or, alternatively, could undergo transmetalation to form an aryl Ni(I)], calculations show that these systems share the same critical C(sp^2)−C(sp^3) formation step!

The reactivity of different alkyl radicals was also compared in the Ni-bipyridine system. This information suggests that relatively subtle changes in the alkyl radical precursors and ligands have a dramatic effect on the mechanism of the reactions. Nonetheless, this investigation sheds light on mechanistic possibilities that were never considered previously and inspires the design of catalytic systems and modification of substrates for Ni-catalyzed C(sp^2)−C(sp^3) cross-coupling reactions. Further exploration will be focused on the comparison of more neutral and anionic ligand systems and the behavior of different alkyl radicals based on the mechanistic models proposed here.

■ ASSOCIATED CONTENT

Supporting Information

The Supporting Information is available free of charge at https://pubs.acs.org/doi/10.1021/jacs.0c02355.

Experimental and computational details, coordinates, and spectral data (PDF)

■ AUTHOR INFORMATION

Corresponding Authors

Osvaldo Gutierrez − *Department of Chemistry and Biochemistry, University of Maryland, College Park, Maryland 20742, United States;* orcid.org/0000-0001-8151-7519; Email: ogs@umd.edu

Gary A. Molander − *Roy and Diana Vagelos Laboratories, Department of Chemistry, University of Pennsylvania, Philadelphia, Pennsylvania 19104-6323, United States;* orcid.org/0000-0002-9114-5584; Email: gmolandr@sas.upenn.edu

Authors

Mingbin Yuan − *Department of Chemistry and Biochemistry, University of Maryland, College Park, Maryland 20742, United States*

Zhihui Song − *Department of Chemistry and Biochemistry, University of Maryland, College Park, Maryland 20742, United States*

Shorouk O. Badir − *Roy and Diana Vagelos Laboratories, Department of Chemistry, University of Pennsylvania, Philadelphia, Pennsylvania 19104-6323, United States*

Complete contact information is available at: https://pubs.acs.org/10.1021/jacs.0c02355

Author Contributions

‡M. Yuan and Z. Song contributed equally.

Notes

The authors declare no competing financial interest.

■ ACKNOWLEDGMENTS

We are grateful for the financial support by the NSF (CAREER 1751568). O.G. is grateful to the University of Maryland College Park for start-up funds and computational resources from UMD Deepthought2 and MARCC/BlueCrab HPC clusters and XSEDE (CHE160082 and CHE160053). G.M. thanks the National Institutes of General Medical Sciences for support (R35 GM 131680).

https://dx.doi.org/10.1021/jacs.0c02355
J. Am. Chem. Soc. 2020, 142, 7225−7234

REFERENCES

(1) de Meijere, A., Braše, S., Oestreich, M., Eds. *Metal-Catalyzed Cross-Coupling Reactions and More*; Wiley-VCH Verlag GmbH: Weinheim, 2014.

(2) (a) Cho, C. H.; Yun, H. S.; Park, K. Nickel(0)-Catalyzed Cross-Coupling of Alkyl Arenesulfonates with Aryl Grignard Reagents. *J. Org. Chem.* **2003**, *68*, 3017−3025. (b) Cheng, Y.; Wu, Y.; Tan, G.; You, J. Nickel Catalysis Enables Oxidative C(sp2)-H/C(sp2)-H Cross-Coupling Reactions between Two Heteroarenes. *Angew. Chem., Int. Ed.* **2016**, *55*, 12275−12279.

(3) (a) Quasdorf, K. W.; Overman, L. E. Catalytic enantioselective synthesis of quaternary carbon stereocentres. *Nature* **2014**, *516*, 181−191. (b) Das, J. P.; Marek, I. Enantioselective synthesis of all-carbon quaternary stereogenic centers in acyclic systems. *Chem. Commun.* **2011**, *47*, 4593−4623. (c) Christoffers, J.; Baro, A. Stereoselective Construction of Quaternary Stereocenters. *Adv. Synth. Catal.* **2005**, *347*, 1473−1482.

(4) Lohre, C.; Dröge, T.; Wang, C.; Glorius, F. Nickel-Catalyzed Cross-Coupling of Aryl Bromides with Tertiary Grignard Reagents Utilizing Donor-Functionalized N-Heterocyclic Carbenes (NHCs). *Chem. - Eur. J.* **2011**, *17*, 6052−6055.

(5) Joshi-Pangu, A.; Wang, C.-Y.; Biscoe, M. R. Nickel-Catalyzed Kumada Cross-Coupling Reactions of Tertiary Alkylmagnesium Halides and Aryl Bromides/Triflates. *J. Am. Chem. Soc.* **2011**, *133*, 8478−8481.

(6) Zultanski, S. L.; Fu, G. C. Nickel-Catalyzed Carbon−Carbon Bond-Forming Reactions of Unactivated Tertiary Alkyl Halides: Suzuki Arylations. *J. Am. Chem. Soc.* **2013**, *135*, 624−628.

(7) (a) Wang, X.; Wang, S.; Xue, W.; Gong, H. Nickel-Catalyzed Reductive Coupling of Aryl Bromides with Tertiary Alkyl Halides. *J. Am. Chem. Soc.* **2015**, *137*, 11562−11565. (b) Wang, X.; Ma, G.; Peng, Y.; Pitsch, C. E.; Moll, B. J.; Ly, T. D.; Wang, X.; Gong, H. Ni-Catalyzed Reductive Coupling of Electron-Rich Aryl Iodides with Tertiary Alkyl Halides. *J. Am. Chem. Soc.* **2018**, *140*, 14490−14497.

(8) Zhou, Q.; Cobb, K. M.; Tan, T.; Watson, M. P. Stereospecific Cross Couplings To Set Benzylic, All-Carbon Quaternary Stereocenters in High Enantiopurity. *J. Am. Chem. Soc.* **2016**, *138*, 12057−12060.

(9) Primer, D. N.; Molander, G. A. Enabling the Cross-Coupling of Tertiary Organoboron Nucleophiles through Radical-Mediated Alkyl Transfer. *J. Am. Chem. Soc.* **2017**, *139*, 9847−9850.

(10) (a) Chen, T.; Zhang, H.; Mykhailiuk, P. K.; Merchant, R. R.; Smith, C. A.; Qin, T.; Baran, P. S. Quaternary Centers by Nickel-Catalyzed Cross-Coupling of Tertiary Carboxylic Acids and (Hetero)-Aryl Zinc Reagents. *Angew. Chem., Int. Ed.* **2019**, *58*, 2454−2458. (b) Green, S. A.; Huffman, T. R.; McCourt, R. O.; Puyl, V.; Shenvi, R. A. Hydroalkylation of Olefins To Form Quaternary Carbons. *J. Am. Chem. Soc.* **2019**, *141*, 7709−7714.

(11) (a) Tellis, J. C.; Primer, D. N.; Molander, G. A. Single-electron transmetalation in organoboron cross-coupling by photoredox/nickel dual catalysis. *Science* **2014**, *345*, 433−436. (b) Tellis, J. C.; Kelly, C. B.; Primer, D. N.; Jouffroy, M.; Patel, N. R.; Molander, G. A. Single-Electron Transmetalation via Photoredox/Nickel Dual Catalysis: Unlocking a New Paradigm for sp3−sp2 Cross-Coupling. *Acc. Chem. Res.* **2016**, *49*, 1429−1439. (c) Primer, D. N.; Karakaya, I.; Tellis, J. C.; Molander, G. A. Single-Electron Transmetalation: An Enabling Technology for Secondary Alkylboron Cross-Coupling. *J. Am. Chem. Soc.* **2015**, *137*, 2195−2198.

(12) For recent reviews, see: (a) Sperger, T.; Sanhueza, I. A.; Kalvet, I.; Schoenebeck, F. Computational Studies of Synthetically Relevant Homogeneous Organometallic Catalysis Involving Ni, Pd, Ir, and Rh: An Overview of Commonly Employed DFT Methods and Mechanistic Insights. *Chem. Rev.* **2015**, *115*, 9532−9586. (b) Vogiatzis, K. D.; Polynski, M. V.; Kirkland, J. K.; Townsend, J.; Hashemi, A.; Liu, C.; Pidko, E. A. Computational Approach to Molecular Catalysis by 3d Transition Metals: Challenges and Opportunities. *Chem. Rev.* **2019**, *119*, 2453−2523.

(13) For selected examples on computational analysis of nickel-catalyzed reactions, see: (a) Oshita, H.; Suzuki, T.; Kawashima, K.; Abe, H.; Tani, F.; Mori, S.; Yajima, T.; Shimazaki, Y. The effect of $\pi-\pi$ stacking interaction of the indole ring with the coordinated phenoxyl radical in a nickel(II)-salen type complex. Comparison with the corresponding Cu(II) complex. *Dalton Trans.* **2019**, *48*, 12060−12069. (b) Slater, J. W.; Marguet, S. C.; Cirino, S. L.; Maugeri, P. T.; Shafaat, H. S. Experimental and DFT Investigations Reveal the Influence of the Outer Coordination Sphere on the Vibrational Spectra of Nickel- Substituted Rubredoxin, a Model Hydrogenase Enzyme. *Inorg. Chem.* **2017**, *56*, 3926−3938. (c) Matsui, J. K.; Gutierrez-Bonet, A.; Rotella, M.; Alam, R.; Gutierrez, O.; Molander, G. A. Photoredox/Nickel-Catalyzed Single-Electron Tsuji−Trost Reaction: Development and Mechanistic Insights. *Angew. Chem.* **2018**, *130*, 16073−16077. (d) Dohm, S.; Hansen, A.; Steinmetz, M.; Grimme, S.; Checinski, M. P. Comprehensive Thermochemical Benchmark Set of Realistic Closed-Shell Metal Organic Reactions. *J. Chem. Theory Comput.* **2018**, *14*, 2596−2608. (e) Yin, H.; Fu, G. C. Mechanistic Investigation of Enantioconvergent Kumada Reactions of Racemic α-Bromoketones Catalyzed by a Nickel/Bix(oxazoline) Complex. *J. Am. Chem. Soc.* **2019**, *141*, 15433−15440.

(14) For an example of nickel-catalyzed transformations via an outer-sphere pathway, see: Jiang, J.; Fu, M.; Li, C.; Shang, R.; Fu, Y. Theoretical Investigation on Nickel-Catalyzed Hydrocarboxylation of Alkynes Employing Formic Acid. *Organometallics* **2017**, *36*, 2818−2825.

(15) (a) Luo, Y.; Gutierrez-Bonet, A.; Matsui, J. K.; Rotella, M. E.; Dykstra, R.; Gutierrez, O.; Molander, G. A. Oxa- and Azabenzonorbornadienes as Electrophilic Partners under Photoredox/Nickel Dual Catalysis. *ACS Catal.* **2019**, *9*, 8835−8842. (b) Desrosiers, J. N.; Wei, X.; Gutierrez, O.; Savoie, J.; Qu, B.; Zeng, X.; Lee, H.; Grinberg, N.; Haddad, N.; Yee, N. K.; Roschangar, F.; Song, J. J.; Kozlowski, M. C.; Senanayake, C. H. Nickel-catalyzed C-3 direct arylation of pyridinium ions for the synthesis of 1-azafluorenes. *Chem. Sci.* **2016**, *7*, 5581−5586.

(16) Shu, W.; Garcia-Dominguez, A.; Quirós, M. T.; Mondal, R.; Cardenas, D. J.; Nevado, C. Ni-Catalyzed Reductive Dicarbofunctionalization of Nonactivated Alkenes: Scope and Mechanistic Insights. *J. Am. Chem. Soc.* **2019**, *141*, 13812−13821.

(17) Gutierrez, O.; Tellis, J. C.; Primer, D. N.; Molander, G. A.; Kozlowski, M. C. Nickel-Catalyzed Cross-Coupling of Photoredox-Generated Radicals: Uncovering a General Manifold for Stereoconvergence in Nickel-Catalyzed Cross-Couplings. *J. Am. Chem. Soc.* **2015**, *137*, 4896−4899.

(18) Green, S. A.; Vasquez-Cespedes, S.; Shenvi, R. Iron−Nickel Dual-Catalysis: A New Engine for Olefin Functionalization and the Formation of Quaternary Centers. *J. Am. Chem. Soc.* **2018**, *140*, 11317−11324.

(19) Identification of geometry is based on the average angle of the corresponding Ni species; see Figure S10 in the Supporting Information for details.

(20) (a) Liu, L.; Lee, W.; Zhou, J.; Bandyopadhyay, S.; Gutierrez, O. Radical-clock a-halo-esters as mechanistic probes for bisphosphineiron-catalyzed cross-coupling reactions. *Tetrahedron* **2019**, *75*, 129−136. (b) Liu, L.; Lee, W.; Yuan, M.; Gutierrez, O. Mechanisms of Bisphosphine Iron-Catalyzed C(sp2)-C(sp3) Cross-Coupling Reactions: Inner-Sphere or Outer-Sphere Arylation? *Comments Inorg. Chem.* **2018**, *38*, 210−237. (c) Lee, W.; Zhou, J.; Gutierrez, O. Mechanism of Nakamura's Bisphosphine Iron-Catalyzed Asymmetric C(sp2)-C(sp3) Cross-Coupling Reaction: The Role of Spin in Controlling Arylation Pathway. *J. Am. Chem. Soc.* **2017**, *139*, 16126−16133.

(21) Calculations using other substrates and different methods led to the same conclusions (see Figure S3 in the Supporting Information).

(22) For selected examples, see: (a) Qin, T.; Cornella, J.; Li, C.; Malins, L. R.; Edwards, J. T.; Kawamura, S.; Maxwell, B. D.; Eastgate, M. D.; Baran, P. S. A General Alkyl-Alkyl Cross-Coupling Enabled by Redox-active Esters and Alkylzinc Reagents. *Science* **2016**, *352*, 801−805. (b) Gu, J.-W.; Min, Q.-Q.; Yu, L.-C.; Zhang, X. Tandem Difluoroalkylation-Arylation of Enamides Catalyzed by Nickel. *Angew. Chem., Int. Ed.* **2016**, *55*, 12270−12274. (c) Campbell, M. W.;

https://dx.doi.org/10.1021/jacs.0c02355
J. Am. Chem. Soc. 2020, 142, 7225−7234

Compton, J. S.; Kelly, C. B.; Molander, G. A. Three-Component Olefin Dicarbofunctionalization Enabled by Nickel/Photoredox Dual Catalysis. *J. Am. Chem. Soc.* **2019**, *141*, 20069−20078.

(23) We investigated the possibility of ligand dissociation from a Ni(III) intermediate, which might invoke structural rearrangement of Ni(III) intermediates. However, based on our calculations the complete ligand dissociation is unlikely to occur on neither ^{2}**H** nor ^{2}**H′** since these processes are both uphill in energy (see Figure S19 for energetic details in the Supporting Information). In addition, although transient decoordination of one of the pyridine ligands was observed in quasi-classical dynamics simulations on ^{2}**K-TS** in the forward direction (see Figure S20 for an example trajectory), the Ni(III) intermediates did not undergo any structural rearrangement, but rather kept the same conformation until the end of the simulation (60% of trajectories) or underwent radical dissociation of the *t*-Bu radical from the axial position of the Ni center (40% of trajectories).

(24) For selected reviews, see: (a) Diccianni, J. B.; Diao, T. Mechanisms of Nickel-Catalyzed Cross-Coupling Reactions. *Trends in Chemistry.* **2019**, *1*, 830−844. (b) Shi, R.; Zhang, Z.; Hu, X. Nickamine and Analogous Nickel Pincer Catalysts for Cross-Coupling of Alkyl Halides and Hydrosilylation of Alkenes. *Acc. Chem. Res.* **2019**, *52*, 1471−1483. (c) Feng, Z.; Xiao, Y.; Zhang, X. Transition-Metal (Cu, Pd, Ni)-Catalyzed Difluoroalkylation via Cross-Coupling with Difluoroalkyl Halides. *Acc. Chem. Res.* **2018**, *51*, 2264−2278. (d) Gu, J.; Wang, X.; Xue, W.; Gong, H. Nickel-catalyzed reductive coupling of alkyl halides with other electrophiles: concept and mechanistic considerations. *Org. Chem. Front.* **2015**, *2*, 1411−1421. (e) Hu, X. Nickel-catalyzed cross coupling of non-activated alkyl halides: a mechanistic perspective. *Chem. Sci.* **2011**, *2*, 1867−1886.

(25) Further calculations suggest that these side reactions are feasible in the reaction system, which could explain the observation of THF-Ar adduct and Ar-H in the stoichiometric studies of aryl bromo Ni(II) with *t*-Bu-BF_3K in experiment (see Figures S11 and S12 in the Supporting Information for the calculation of possible side reaction pathways).

(26) For reviews, see: (a) Ess, D. H.; Houk, K. N. Distortion/Interaction Energy Control of 1,3-Dipolar Cycloaddition Reactivity. *J. Am. Chem. Soc.* **2007**, *129*, 10646−10647. (b) Ess, D. H.; Houk, K. N. Theory of 1,3-Dipolar Cycloadditions: Distortion/Interaction and Frontier Molecular Orbital Models. *J. Am. Chem. Soc.* **2008**, *130*, 10187−10198. (c) Fernandez, I.; Bickelhaupt, F. M. The activation strain model and molecular orbital theory: understanding and designing chemical reactions. *Chem. Soc. Rev.* **2014**, *43*, 4953−4967. (d) Wolters, L. P.; Bickelhaupt, F. M. The activation strain model and molecular orbital theory. *Wiley Interdisciplinary Reviews: Computational Molecular Science* **2015**, *5*, 324−343.

https://dx.doi.org/10.1021/jacs.0c02355
J. Am. Chem. Soc. 2020, 142, 7225−7234